Neural Representations of Location Composed of Spatially Periodic Bands

Julija Krupic *et al.*

Science **337**, 853 (2012);
DOI: 10.1126/science.1222403

not propagate to the soma to yield place-field activity. However, a spatially uniform signal that slightly depolarizes the soma can reveal this input. This gating of inputs, as opposed to just outputs, by somatic V_m constitutes a novel mechanism for receptive fields. It also implies that integration of multiple inputs is gated by somatic V_m (fig. S10).

These results are the opposite of those expected from standard models of cortical receptive fields (*22*, *23*) and place cells (*7*–*11*). In these models, a neuron receives more excitatory synaptic input in response to the preferred stimulus, and this input is passively summed then compared with the AP threshold. Silent cells would have spatially tuned somatic V_m hills of various amplitudes that do not reach threshold, and somatic depolarization would reduce the driving force and, thus, hill amplitude (*23*).

At the other extreme is a model in which synaptic inputs are uniformly distributed in stimulus space, and the neuron selectively amplifies a subset of them. This possibility is supported by recent in vivo work in visual cortex showing that input signals coding for multiple stimulus orientations are present in each neuron, regardless of its output tuning (*24*), and in vitro work showing that particular dendrites can propagate inputs to the soma more effectively than others (*25*) via dendritic spiking (*15*, *16*, *25*, *26*).

Our results strongly support such nonlinear dendritic amplification mechanisms, regardless of whether synaptic inputs are uniformly distributed. In particular, in vitro work has shown that depolarizing the somatic (*27*, *28*) or dendritic (*29*) V_m can gate inputs in a thresholdlike manner. The lack of a hill or increased fluctuations at resting V_m makes unlikely a purely somatic locus of amplification. Rather, somatic depolarization may (i) shift the dendritic V_m closer to the activation range of voltage-gated conductances or deactivate hyperpolarization-activated currents (increasing R_N locally), and thus amplify spatially tuned responses and trigger dendritic spikes, or (ii) simply push the peak response in the dendrite above the dendritic spike threshold. Or instead, depolarization may act to let already existing dendritic spikes propagate to the soma (*29*).

These findings have important implications for place cells, spatial memory, and hippocampal-dependent memory in general. In novel environments, inhibitory neuron activity drops (*30*), which could depolarize the somatic baseline V_m of a silent cell and produce place fields (*30*, *31*) without requiring synaptic plasticity. Neuromodulation could also cause depolarization or lower the threshold baseline $V_{m,gate}$ described here. Furthermore, already existing place cells could be those neurons whose $V_{m,gate}$ is below their baseline V_m. That is, (baseline $V_m - V_{m,gate}$) could reflect intrinsic excitability, with depolarization compensating for lower excitability in silent cells. Alternatively, place cell inputs could differ or be arranged differently on the dendritic tree, although this would not easily explain preexploration differences in excitability (*14*). Finally, the explicit demonstration that most CA1 pyramidal neurons, even originally silent ones, can be place cells in a given maze suggests that the role of CA1 is not only to create spatial tuning, but to choose which subset of neurons should be active within a specific environment. The exclusively input-based models of place cells (*7*–*11*) could work as described but with an independent, excitability-based "AND" gate added. The distribution of excitability levels across the population would then determine which cells would represent a new item or environment in memory (*14*, *32*). Moreover, the gating machinery would be a potential locus of plasticity for long-term storage (*25*–*29*).

References and Notes

1. J. O'Keefe, L. Nadel, *The Hippocampus as a Cognitive Map* (Clarendon Press, Oxford, 1978).
2. J. O'Keefe, J. Dostrovsky, *Brain Res.* **34**, 171 (1971).
3. L. T. Thompson, P. J. Best, *J. Neurosci.* **9**, 2382 (1989).
4. R. Q. Quiroga, L. Reddy, G. Kreiman, C. Koch, I. Fried, *Nature* **435**, 1102 (2005).
5. T. Hafting, M. Fyhn, S. Molden, M.-B. Moser, E. I. Moser, *Nature* **436**, 801 (2005).
6. V. Chevaleyre, S. A. Siegelbaum, *Neuron* **66**, 560 (2010).
7. M. V. Tsodyks, T. J. Sejnowski, *Int. J. Neural Syst.* **6**, 81 (1995).
8. N. Burgess, J. O'Keefe, *Hippocampus* **6**, 749 (1996).
9. A. Samsonovich, B. L. McNaughton, *J. Neurosci.* **17**, 5900 (1997).
10. T. Solstad, E. I. Moser, G. T. Einevoll, *Hippocampus* **16**, 1026 (2006).
11. L. de Almeida, M. Idiart, J. E. Lisman, *J. Neurosci.* **29**, 7504 (2009).
12. A. K. Lee, J. Epsztein, M. Brecht, *Soc. Neurosci. Abstr.* **2008**, 690.22 (2008).
13. C. D. Harvey, F. Collman, D. A. Dombeck, D. W. Tank, *Nature* **461**, 941 (2009).
14. J. Epsztein, M. Brecht, A. K. Lee, *Neuron* **70**, 109 (2011).
15. M. Häusser, N. Spruston, G. J. Stuart, *Science* **290**, 739 (2000).
16. D. Johnston, R. Narayanan, *Trends Neurosci.* **31**, 309 (2008).
17. A. K. Lee, I. D. Manns, B. Sakmann, M. Brecht, *Neuron* **51**, 399 (2006).
18. A. K. Lee, J. Epsztein, M. Brecht, *Nat. Protoc.* **4**, 385 (2009).
19. V. H. Brun *et al.*, *Science* **296**, 2243 (2002).
20. V. H. Brun *et al.*, *Neuron* **57**, 290 (2008).
21. T. Nakashiba, J. Z. Young, T. J. McHugh, D. L. Buhl, S. Tonegawa, *Science* **319**, 1260 (2008).
22. N. J. Priebe, D. Ferster, *Neuron* **57**, 482 (2008).
23. S. Crochet, J. F. A. Poulet, Y. Kremer, C. C. H. Petersen, *Neuron* **69**, 1160 (2011).
24. H. Jia, N. L. Rochefort, X. Chen, A. Konnerth, *Nature* **464**, 1307 (2010).
25. A. Losonczy, J. K. Makara, J. C. Magee, *Nature* **452**, 436 (2008).
26. N. L. Golding, N. Spruston, *Neuron* **21**, 1189 (1998).
27. D.-S. Wei *et al.*, *Science* **293**, 2272 (2001).
28. G. Major, A. Polsky, W. Denk, J. Schiller, D. W. Tank, *J. Neurophysiol.* **99**, 2584 (2008).
29. T. Jarsky, A. Roxin, W. L. Kath, N. Spruston, *Nat. Neurosci.* **8**, 1667 (2005).
30. M. A. Wilson, B. L. McNaughton, *Science* **261**, 1055 (1993).
31. L. M. Frank, G. B. Stanley, E. N. Brown, *J. Neurosci.* **24**, 7681 (2004).
32. Y. Zhou *et al.*, *Nat. Neurosci.* **12**, 1438 (2009).

Acknowledgments: We would like to thank G. Shtengel, J. Osborne, L. Ramasamy, D. Cabaniss, S. Bassin, C. Werner, B. Shields, A. Hu, M. J. Kim, H.-P. Liaw, G. Crosby, and D. Culley for technical advice and assistance and J. Dudman, N. Spruston, G. Murphy, J. Magee, K. Svoboda, J. Cohen, and D. Rich for valuable discussions about the manuscript. This work was supported by the Howard Hughes Medical Institute.

Supplementary Materials

www.sciencemag.org/cgi/content/full/337/6096/849/DC1
Materials and Methods
Figs. S1 to S10
References

6 March 2012; accepted 18 June 2012
10.1126/science.1221489

Neural Representations of Location Composed of Spatially Periodic Bands

Julija Krupic,[1] Neil Burgess,[2,3] John O'Keefe[1,4]*

The mammalian hippocampal formation provides neuronal representations of environmental location, but the underlying mechanisms are poorly understood. Here, we report a class of cells whose spatially periodic firing patterns are composed of plane waves (or bands) drawn from a discrete set of orientations and wavelengths. The majority of cells recorded in parasubicular and medial entorhinal cortices of freely moving rats belonged to this class and included grid cells, an important subset that corresponds to three bands at 60° orientations and has the most stable firing pattern. Occasional changes between hexagonal and nonhexagonal patterns imply a common underlying mechanism. Our results indicate a Fourier-like spatial analysis underlying neuronal representations of location, and suggest that path integration is performed by integrating displacement along a restricted set of directions.

Grid cells represent the animal's location by firing in a hexagonally symmetric array of locations covering the entire environment (*1*). These cells are found in the medial entorhinal cortex (mEC) (*1*, *2*) and in pre- and parasubiculum (PaS) (*2*). This spatially periodic firing may provide the spatial metric for the hippocampal cognitive map (*3*–*6*). The hexagonal symmetry raises important questions: Is this an entirely unique pattern or one end of a continuum? Is this pattern required for spatial representation, or does it reflect properties such as stability (*7*) or coding efficiency (*8*)? We recorded 351 cells from superficial layers (II and III) of the medial part of dorsocaudal mEC (five implants) and adjacent PaS (two implants) in seven adult male rats (fig. S1) while they foraged for food in a square enclosure (1.69 m^2). Many of these showed the regular hexagonal

[1]Department of Cell and Developmental Biology, University College London (UCL), London WC1E 6BT, UK. [2]Institute of Cognitive Neuroscience, UCL, 17 Queen Square, London WC1N 3AR, UK. [3]Institute of Neurology, UCL, Queen Square, London WC1N 3BG, UK. [4]Sainsbury-Wellcome Centre for Neural Circuits and Behaviour, UCL, London WC1E 6BT, UK.

*To whom correspondence should be addressed: E-mail: j.okeefe@ucl.ac.uk

pattern characteristic of grid cells [26% passed the standard "gridness" measure (*1*)] (Fig. 1A), but a surprisingly large portion (44%) had stable multipeaked patterns lacking the signature hexagonal symmetry (Fig. 1, B and C).

We used two-dimensional (2D) Fourier spectral analysis to identify cells whose spatial firing patterns showed significant spatial periodicity (*9*), being predominantly composed of a small number of Fourier components (that is, periodic spatial bands with different wavelengths and orientations that sum to produce the firing-rate map) (Fig. 1F). A cell was categorized as spatially periodic if its strongest Fourier component exceeded 95% of those in spatially shuffled data (fig. S2). Overall, 70% of cells were spatially periodic (Fig. 1E and fig. S3, all cells). Of these, 37% were grid cells, which usually have three main Fourier components with similar wavelengths, oriented at multiples of 60° from each other (Fig. 1, F and G, and figs. S4 to S8). The remaining spatially periodic cells had one to four main Fourier components with a greater range of relative orientations and wavelengths (Fig. 1G, figs. S6 and S7, and see fig. S8 for comparability of physiological properties). Spatial periodicity might reflect local rather than global spatial structure in the multipeaked firing fields. Accordingly, we used a second shuffling technique based on shuffling local peak-centered segments of the data. The results show that 144 of 154 (94%) spatially periodic nongrid cells and 89 of 91 (98%) grid cells had significantly more spatially periodic firing patterns than the $P = 0.05$ level in these shuffled data [that is, significantly more global periodicity than predicted by their local spatial structure ($P < 0.01$, binomial probability distribution) (fig. S9) (*9*)]. Several cells with one or two main Fourier components (for example, see Fig. 1C and fig. S10) were reminiscent of the band cells postulated as inputs to grid cells in some computational models [(*7*, *10*), see also (*11*–*13*)].

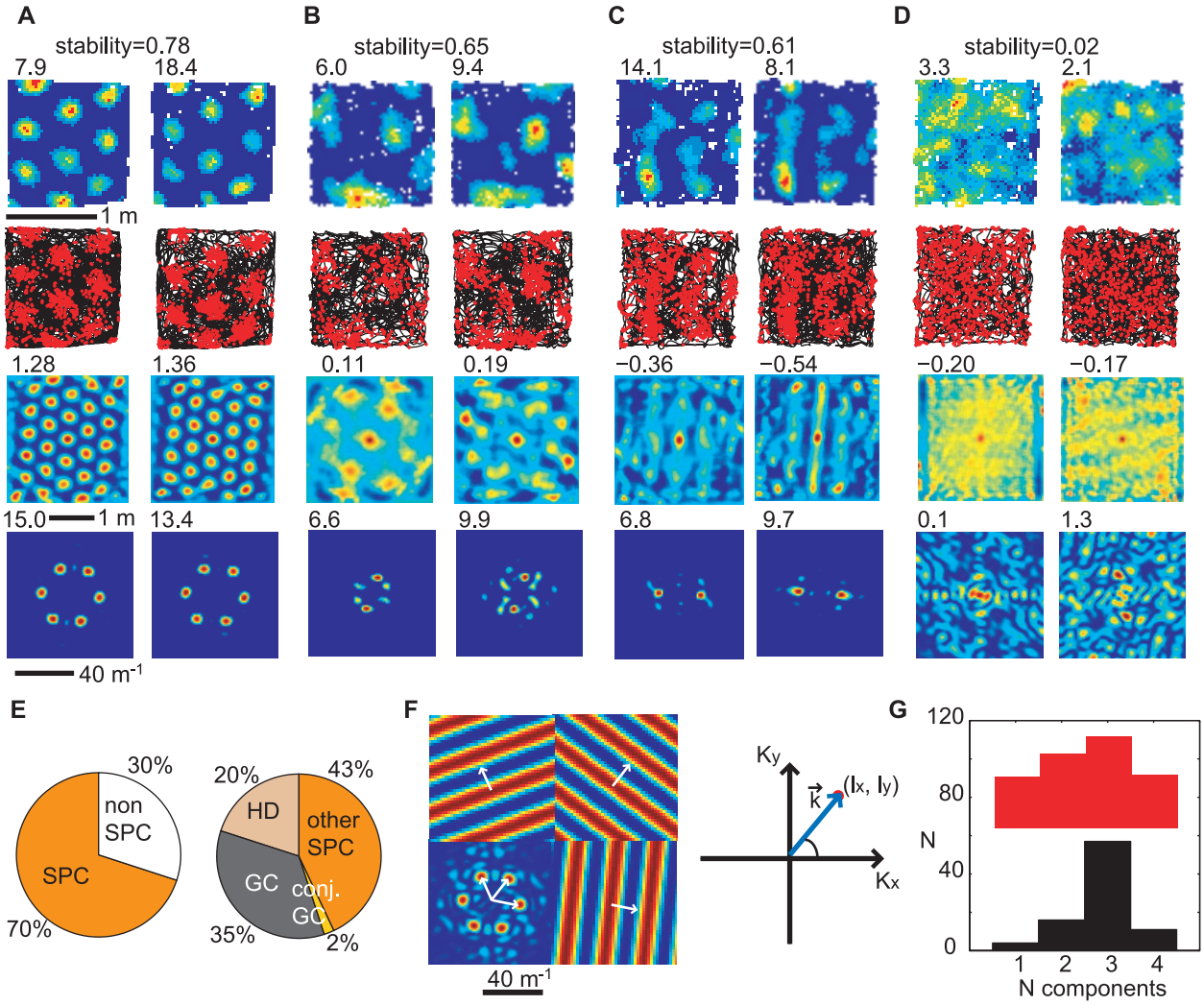

Fig. 1. Spatial periodicity of neuronal firing patterns. (**A** to **D**) Firing-rate maps (top row), trajectory (black) with spike positions (red) (second row), spatial autocorrelograms (third row), and 2D Fourier spectrograms (bottom row) for two successive trials of the same cell in a 1.3- by 1.3-m^2 enclosure. (A to C) Spatially periodic cells. The cell in (A) qualifies as a grid cell, the cell in (B) fires in an irregular grid, and that in (C) has a more bandlike firing pattern. (D) A non spatially periodic cell. Peak firing rate, gridness, and maximum Fourier power are shown (top left of the corresponding plots). Rate-map stability between trials is indicated above. (**E**) Distribution of cell types in dorsal mEC and adjacent PaS. (Left) All cells, divided into spatially periodic (SPC) and non–spatially periodic (nonSPC) cells. (Right) Spatially periodic cells only, divided into grid cells (GC), conjunctive grid cells (conj. GC), SPCs with a head-direction correlate (HD), and other SPCs. (**F**) Two-dimensional Fourier analysis. (Left) The centered 2D Fourier spectrogram of the rate map shown at left in (A), with the main Fourier components shown at the sides with corresponding wave vectors (white arrows). (Right) The spectrogram shows the power corresponding to plane waves (wave vector **k**) at (lx, ly) from the center. The periodic bands in the plane wave are oriented perpendicular to the wave vector **k**, and their wavelength is inversely proportional to its length. (**G**) Distribution of the number of main Fourier components across spatially periodic cells (nongrid cells shown in red, grid cells in black).

Could the spatially periodic nongrid cells provide a consistent metric for an environment comparable to the grid cells? First, we looked at the stability of their firing patterns in familiar environments, between successive trials on the same day and between trials on different days. Spatially periodic nongrid cell firing patterns were significantly more stable than chance, both within and between days. However, grid-cell firing patterns were even more stable than nongrid spatially periodic cells on both comparisons (Fig. 2A). The greater stability of grid-cell firing patterns corresponded to greater stability in the orientations of their Fourier components (Fig. 2B), suggesting a causal relationship between the two.

Some spatially periodic cells (11%) changed their firing patterns from grids to nongrids or vice versa between trials in the same environment (figs. S11 and S12 and table S1). Figure 2C shows an example of a cell whose firing pattern changed from gridlike to bandlike (a simultaneously recorded grid cell remained unchanged, see fig. S12 for details). Such transitions did not reflect unidirectional drift of the grid pattern (sliding time-window spatial autocorrelation analysis) (fig. S13). These transitions suggest a continuous population of spatially periodic cells, with grids and nongrids reflecting different combinations of a small set of elemental periodic bands.

A larger proportion of spatially periodic cells (32%) changed between grids and nongrids across different environments (Fig. 2D and table S1), although the majority did not change category (Fig. 2, E and F). These transitions corresponded to changing configurations of underlying periodic bands. They did not reflect simpler transformations previously reported for grid cells after environmental manipulations [rotations and translations (*14*), rescaling (*15*), or expansions (*16*)].

Are the spatially periodic cells in one animal composed from the same set of bands? All of these cells tended to have Fourier components clustered around a small number of orientations and wavelengths (figs. S5 to S7) (*15*). As expected, grid-cell components were aligned (*15*, *17*) and oriented at 60° to each other (Fig. 3, A to G; Rayleigh vector $R_0 = 0.58 \pm 0.14$ for clustering modulo 60°, $P < 0.01$), corroborated by a clustering of the angular separation of neighboring components around 60° (Fig. 3H; Rayleigh vector $R_0 = 1.1$, $P < 0.001$). The orientations of components of spatially periodic nongrid cells tended to align with those of grid cells (Fig. 3, A to G, and fig. S5; mean correlation coefficient of 0.54 ± 0.08, $P < 0.01$ from shuffled data) but included a wider range of relative orientations (Fig. 3I).

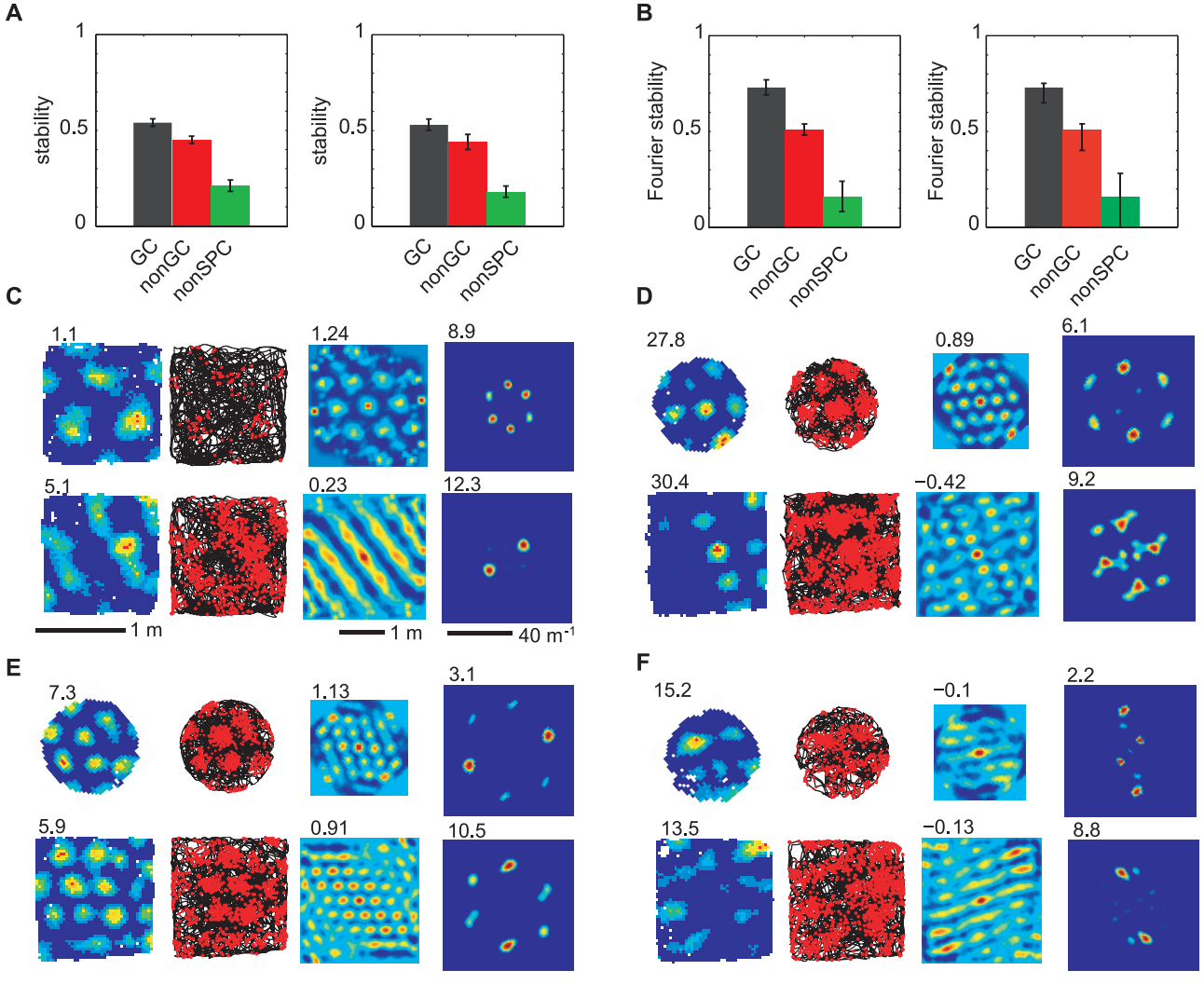

Fig. 2. Stability of spatially periodic cell firing. (**A**) Grid cells were more stable than spatially periodic nongrid cells (nonGC), and both were superior to nonspatially periodic cells, both between sessions on the same day in the same environment [(left) GC: correlation coefficient $r = 0.54 \pm 0.02$ (mean ± SEM), nonGC: $r = 0.45 \pm 0.02$, nonSPC: $r = 0.21 \pm 0.03$, P_{144}(GC > nonGC) = 0.015, P_{78}(GC > nonSPC) = 0.65E−012, P_{125}(nonGC > nonSPC) = 1.69E−010, paired *t* tests, one-tailed] and across days [(right) GC: $r = 0.53 \pm 0.03$, nonGC: $r = 0.44 \pm 0.04$, nonSPC: $r = 0.1\,8 \pm 0.03$, P_{51}(GC > nonGC) = 0.049, P_{24}(GC > nonSPC) = 1.39E−005, P_{41}(nonGC > nonSPC) = 3.14E−004; paired *t* tests, one-tailed]. (**B**) Fourier polar-component stability mirrored rate-map stability between sessions [(left), GC > nonGC: $r = 0.73 \pm 0.04 > r = 0.51 \pm 0.03$, $P_{144} = 3.24$E−005, paired *t* tests, one-tailed] and between days [(right) 0.70 ± 0.06 versus 0.47 ± 0.07, $P_{24} = 0.015$, paired *t* tests, one-tailed]. Occasionally, cell firing altered between grid and nongrid patterns between trials (**C**) in the same environment or (**D**) in different environments. More often, the structure of grids (**E**) and spatially periodic nongrids (**F**) was maintained across environments.

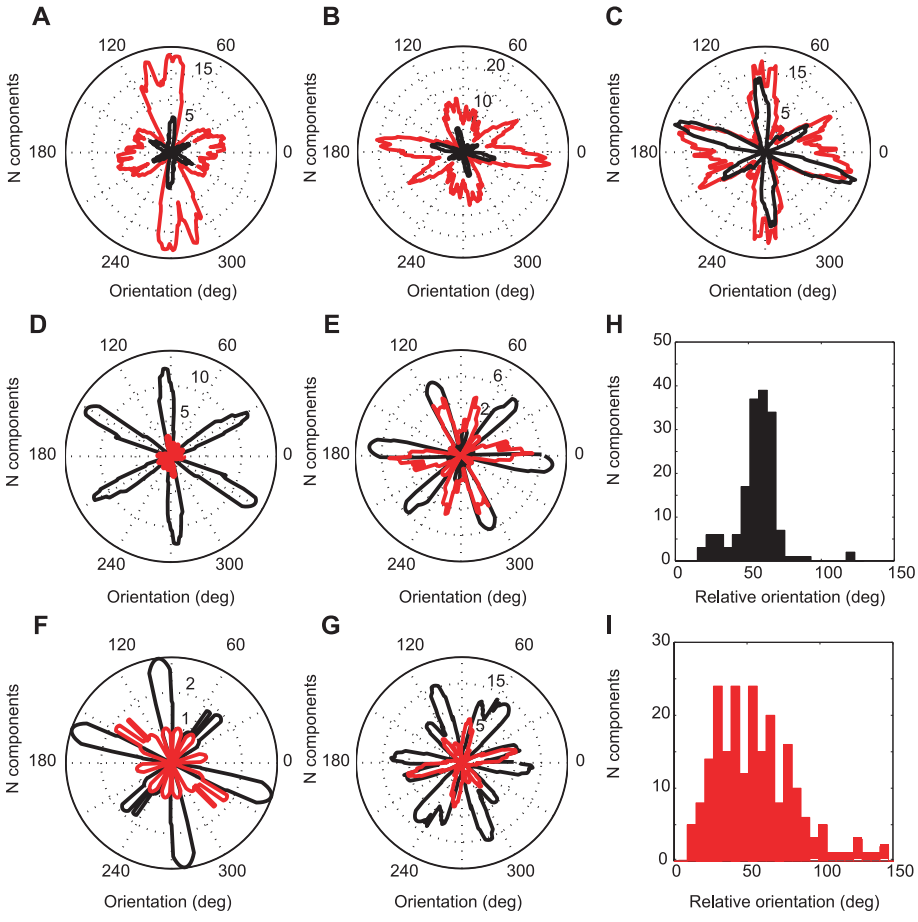

Fig. 3. Orientations of main Fourier components within each animal. (**A** to **G**) Histograms of the orientations of main Fourier components of the spatially periodic cells recorded in each animal (in a 1.3- by 1.3-m^2 enclosure; nongrid cells shown in red, grid cells in black). (A and B) cells in PaS; (C to G) cells in mEC [(A) r1682, (B) r1738, (C) r1728, (D) r1709, (E) r1737, (F) r1739, (G) r1710]. Distributions are shown for the relative orientations of Fourier components of all grid cells (**H**) and all spatially periodic nongrid cells (**I**).

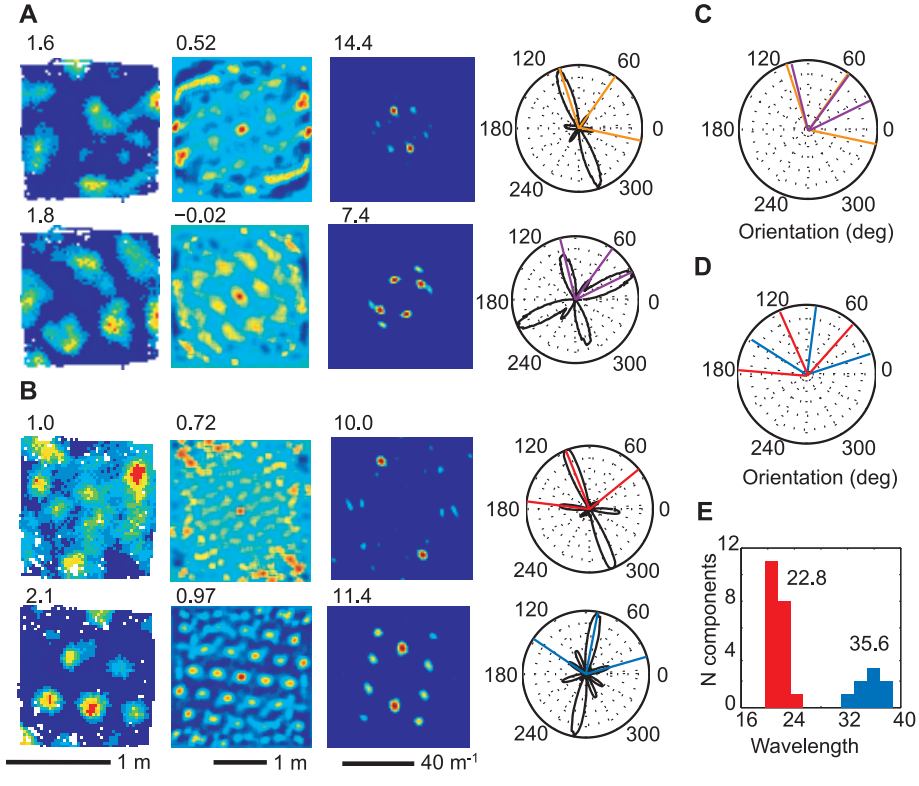

Fig. 4. Spatially periodic cells with different Fourier components coexist within the same animal. (**A**) Simultaneously recorded grid cell (top) and spatially periodic nongrid cell (bottom) with one Fourier component misaligned between the two (r1738). (**B**) Simultaneously recorded grid cells of different scale and orientation (r1737). (Left to right) Firing rate map, spatial autocorrelogram, 2D Fourier spectrogram with peak firing rate, gridness score, and maximum Fourier power indicated on the top-left of the corresponding plots are shown. (**C**) Orientations of the main Fourier components in (A) are superimposed here [colors as in (A)]. (**D**) Mean orientations of the main Fourier components (fig. S15) in (B) [colors as in (B)]. (**E**) Wavelength distribution of Fourier components of simultaneously recorded grid cells with the same orientations as the cell in (B, top; red) and the cell in (B, bottom; blue). The mean wavelength for each module is indicated above. Their ratio is ~1.57.

If grid cells and spatially periodic nongrid cells are composed of subsets from a larger set of bandlike components, there should be examples of simultaneously recorded cells with different components. Figure 4, A and C, shows a grid and nongrid spatially periodic cell differing by ~30° in the orientation of one of their components (see fig. S14 for more examples). Figure 4, B and D, shows two simultaneously recorded grid cells whose three component orientations all differ by ~30° and also differ in wavelengths (see fig. S15 for details).

Finally, we asked whether the proportions of grid and spatially periodic nongrid cells differed between the two anatomical regions investigated. Although the overall percentage of spatially periodic cells was lower in mEC (156/239, 65% in mEC; 89/112, 79% in PaS), the proportion of grid cells in mEC (75/156 or 48%) was much higher than in PaS (16/89 or 18%), despite the close anatomical proximity of these regions (fig. S1). This observation suggests that both regions, with very distinct afferent and efferent connectivity (*2*, *18*, *19*), can generate spatially periodic cells, albeit with major differences in the prevalence of pure hexagonal symmetry. In both regions, cell firing shows strong theta modulation: 67% of all spatially periodic cells were theta-modulated in PaS (mean frequency 9.2 ± 0.1Hz; 65% of all cells were theta-modulated) and 56% in mEC (with similar mean frequency; 47% of all cells were theta-modulated), pointing to a common characteristic of spatially periodic cells regardless of their anatomical location (fig. S16).

The abrupt increase in the proportion of grid cells in mEC suggests that mEC has microcircuitry or anatomical inputs organized to prefer components at 60° angles, which, in turn, provides the most stable inputs to the hippocampus. In contrast, PaS, with a higher proportion of spatially periodic cells but more varied and less stable firing patterns, heavily projects to the superficial layers of mEC (*18*–*20*) and may represent an intermediate stage in constructing stable grids from periodic bands.

The heterogeneous spatially periodic firing patterns reported here could reflect a common process of self-organization acting on band cells upstream of the recorded cells (*7*, *10*). The most stable outcome of such a process would be hexagonal grids (*10*), though mixtures of orientations organized at multiples of around 30° and 60° can also be stable (*7*) and may support multiscale representation (*4*, *21*). What mechanism might underlie the bands? Theta-modulated firing reminds us that theta rhythmicity controls the scale of spatial representations (*22*–*24*) and that interference between theta oscillations could integrate self-motion to produce bandlike firing patterns that drive grid-cell firing (*10*–*12*). These band cells might correspond to phase-modulated firing from theta cells in the septohippocampal circuit (*13*) or may be generated by 1D ring attractors (*7*, *25*). Alternatively, in the attractor model (*4*, *6*, *26*), recurrent interactions between grid cells could produce a stable gridlike, as well as periodic bandlike Turing pattern (*6*, *26*, *27*) of firing across a sheet of cells, which translates into spatial firing as the animal moves.

In summary, the firing patterns of the majority of cells recorded in PaS and mEC showed a stable spatial periodicity described by superposition of a small number (up to four) of elemental periodic bandlike components drawn from a discrete set of orientations and wavelengths. Grid cells correspond to hexagonal configurations, which have the greatest spatial stability. Our results suggest that path integration is performed by integrating self-motion along a restricted set of directions, mediated by planar periodic representations (bands) of multiple scales along each direction, and that self-organization of these bandlike inputs may underlie the firing of all spatially periodic cells in the parahippocampal region.

References and Notes

1. T. Hafting, M. Fyhn, S. Molden, M.-B. Moser, E. I. Moser, *Nature* **436**, 801 (2005).
2. C. N. Boccara *et al*., *Nat. Neurosci.* **13**, 987 (2010).
3. J. O'Keefe, L. Nadel, *The Hippocampus as a Cognitive Map* (Oxford Univ. Press, Oxford, 1978).
4. I. R. Fiete, Y. Burak, T. Brookings, *J. Neurosci.* **28**, 6858 (2008).
5. J. O'Keefe, N. Burgess, *Hippocampus* **15**, 853 (2005).
6. B. L. McNaughton, F. P. Battaglia, O. Jensen, E. I. Moser, M.-B. Moser, *Nat. Rev. Neurosci.* **7**, 663 (2006).
7. H. Mhatre, A. Gorchetchnikov, S. Grossberg, *Hippocampus* **22**, 320 (2012).
8. S. Sreenivasan, I. Fiete, *Nat. Neurosci.* **14**, 1330 (2011).
9. Materials and methods are available as supplementary materials on *Science* Online.
10. N. Burgess, C. Barry, J. O'Keefe, *Hippocampus* **17**, 801 (2007).
11. N. Burgess, *Hippocampus* **18**, 1157 (2008).
12. M. E. Hasselmo, *Hippocampus* **18**, 1213 (2008).
13. A. C. Welday, I. G. Shlifer, M. L. Bloom, K. Zhang, H. T. Blair, *J. Neurosci.* **31**, 16157 (2011).
14. M. Fyhn, T. Hafting, A. Treves, M.-B. Moser, E. I. Moser, *Nature* **446**, 190 (2007).
15. C. Barry, R. Hayman, N. Burgess, K. J. Jeffery, *Nat. Neurosci.* **10**, 682 (2007).
16. C. Barry, J. O'Keefe, N. Burgess, Society for Neuroscience Annual Meeting abstract 35, poster no. 101.24 (Chicago, IL, 17 to 21 October 2009).
17. C. F. Doeller, C. Barry, N. Burgess, *Nature* **463**, 657 (2010).
18. T. van Groen, J. M. Wyss, *Brain Res.* **518**, 227 (1990).
19. A. Burgalossi *et al*., *Neuron* **70**, 773 (2011).
20. C. Köhler, *J. Comp. Neurol.* **236**, 504 (1985).
21. H. T. Blair, A. C. Welday, K. Zhang, *J. Neurosci.* **27**, 3211 (2007).
22. A. P. Maurer, S. R. Vanrhoads, G. R. Sutherland, P. Lipa, B. L. McNaughton, *Hippocampus* **15**, 841 (2005).
23. C. Geisler, D. Robbe, M. Zugaro, A. Sirota, G. Buzsáki, *Proc. Natl. Acad. Sci. U.S.A.* **104**, 8149 (2007).
24. J. O'Keefe, M. L. Recce, *Hippocampus* **3**, 317 (1993).
25. H. T. Blair, K. Gupta, K. Zhang, *Hippocampus* **18**, 1239 (2008).
26. M. C. Fuhs, D. S. Touretzky, *J. Neurosci.* **26**, 4266 (2006).
27. P. Borckmans *et al*., *Int. J. Bifurcat. Chaos* **12**, 2307 (2002).

Acknowledgments: This work was supported by the European Union Framework 7 (SPACEBRAIN) grant, the UK Medical Research Council, the Gatsby Charitable Foundation, and the Wellcome Trust. J.K. received support from a CoMPLEX studentship. We thank M. Bauza, T. Wills, C. Barry, F. Cacucci, and M. Witter for useful discussions and S. Burton for help with histology. This work was conducted in accordance with the UK Animals (Scientific Procedures) Act (1986).

Supplementary Materials

www.sciencemag.org/cgi/content/full/337/6096/853/DC1
Materials and Methods
Figs. S1 to S16
Table S1
References

26 March 2012; accepted 12 June 2012
10.1126/science.1222403

A TOG:αβ-tubulin Complex Structure Reveals Conformation-Based Mechanisms for a Microtubule Polymerase

Pelin Ayaz, Xuecheng Ye, Patrick Huddleston, Chad A. Brautigam, Luke M. Rice*

Stu2p/XMAP215/Dis1 family proteins are evolutionarily conserved regulatory factors that use αβ-tubulin–interacting tumor overexpressed gene (TOG) domains to catalyze fast microtubule growth. Catalysis requires that these polymerases discriminate between unpolymerized and polymerized forms of αβ-tubulin, but the mechanism by which they do so has remained unclear. Here, we report the structure of the TOG1 domain from Stu2p bound to yeast αβ-tubulin. TOG1 binds αβ-tubulin in a way that excludes equivalent binding of a second TOG domain. Furthermore, TOG1 preferentially binds a curved conformation of αβ-tubulin that cannot be incorporated into microtubules, contacting α- and β-tubulin surfaces that do not participate in microtubule assembly. Conformation-selective interactions with αβ-tubulin explain how TOG-containing polymerases discriminate between unpolymerized and polymerized forms of αβ-tubulin and how they selectively recognize the growing end of the microtubule.

Microtubules are highly regulated, dynamic polymers of αβ-tubulin that have essential roles in intracellular organization and chromosome segregation. Microtubules grow faster in vivo than they do in vitro [reviewed in (*1*)]. Proteins in the Stu2p/XMAP215/Dis1 family (*2*–*4*) are the major cellular factors that promote fast microtubule elongation. These proteins contain multiple tumor overexpressed gene (TOG) domains that function as αβ-tubulin binding modules (*5*) and are required for the elongation-promoting activity of this family (*5*, *6*). The

Departments of Biophysics and Biochemistry, University of Texas Southwestern Medical Center, 5323 Harry Hines Blvd, Dallas, TX 75390, USA.

*To whom correspondence should be addressed. E-mail: luke.rice@utsouthwestern.edu